

1 **The influence of clouds on radical concentrations:**
2 **Observations and modelling studies of HO_x during the Hill**
3 **Cap Cloud Thuringia (HCCT) campaign in 2010**

4 **L. K. Whalley^{1,2}, D. Stone², I. J. George^{2,*}, S. Mertes³, D. van Pinxteren³, A.**
5 **Tilgner³, H. Herrmann³, M. J. Evans^{4,5} and D.E. Heard^{1,2}**

6 [1] {National Centre for Atmospheric Science, University of Leeds, Leeds, LS2 9JT, UK}

7 [2] {School of Chemistry, University of Leeds, Leeds, LS2 9JT, UK}

8 [3] {Leibniz-Institut für Troposphärenforschung (TROPOS), Permoserstr. 15, 04318 Leipzig, Germany}

9 [4] {National Centre for Atmospheric Science, University of York, York, YO10 5DD, UK}

10 [5] {Department of Chemistry, University of York, York, YO10 5DD, UK}

11 [*] {Now at National Risk Management Research Laboratory, U.S. Environmental Protection Agency,
12 Research Triangle Park, North Carolina 27711, USA}

13 Correspondence to: L. K. Whalley (l.k.whalley@leeds.ac.uk)

14
15 **Abstract**

16 The potential for chemistry occurring in cloud droplets to impact atmospheric composition
17 has been known for some time. However, the lack of direct observations and uncertainty in
18 the magnitude of these reactions, led to this area being overlooked in most chemistry
19 transport models. Here we present observations from Mt. Schmücke, Germany, of the HO₂
20 radical made alongside a suite of cloud measurements. HO₂ concentrations were depleted in-
21 cloud by up to 90% with the rate of heterogeneous loss of HO₂ to clouds necessary to bring
22 model and measurements into agreement demonstrating a dependence on droplet surface area
23 and pH. This provides the first observationally derived assessment for the uptake coefficient
24 of HO₂ to cloud droplets and was found to be in good agreement with theoretically derived
25 parameterisations. Global model simulations, including this cloud uptake, showed impacts on
26 the oxidizing capacity of the troposphere that depended critically on whether the HO₂ uptake
27 leads to production of H₂O₂ or H₂O.

1
2
3
4
5
6
7
8
9
10
11
12
13
14
15
16
17
18
19
20
21
22
23
24
25
26
27
28
29
30
31
32
33

1 Introduction

Clouds occupy around 15% of the volume of the lower troposphere and can impact atmospheric composition through changes in transport, photolysis, wet deposition and in-cloud oxidation of sulphur. Modelling studies have shown that aqueous phase chemistry can also significantly reduce gaseous HO₂ concentrations by heterogeneous uptake and loss into cloud droplets (Jacob, 1996; Tilgner et al., 2005; Huijnen et al., 2014). This chemistry is predicted to reduce OH and O₃ concentrations also due to the reduction in the gas-phase concentration of HO₂. This in turn, decreases the self-cleansing capacity of the atmosphere and increases the lifetime of many trace gases (Lelieveld and Crutzen, 1990) with impacts for climate and air quality. Aqueous phase models have been developed which combine multiphase chemistry with detailed microphysics (Tilgner et al., 2005), but there are limited experimental field data of gas-phase radical concentrations within clouds to corroborate model predictions of heterogeneous loss of radicals to cloud droplets. There have been a number of aircraft campaigns which have measured OH and HO₂ radical concentrations within clouds (Mauldin et al., 1997; Mauldin et al., 1998; Olson et al., 2004; Commane et al., 2010), often, however, simultaneous observations of cloud droplet number and size distributions (or other key gas-phase radical precursors) were not made during these studies, making it difficult to assess the full impact of clouds on radical concentrations. In general therefore climate and air quality models do not consider this impact of clouds on atmospheric composition.

Within the literature, a wide range of uptake coefficients of HO₂ to liquid and aerosol surfaces have been considered to reproduce observed HO₂ concentrations (e.g. (Sommariva et al., 2004; Haggerstone et al., 2005; Emmerson et al., 2007; Whalley et al., 2010)) with often large uptake coefficients (up to 1 at times) used to reconcile model over-predictions. A wide range of uptake coefficients, not wholly consistent with each other, have been reported from laboratory studies (Abbatt et al., 2012). From measurements conducted in our laboratory, uptake probabilities of HO₂ to sub-micron aerosols were found to be less than 0.02 at room temperature (George et al., 2013) for aqueous aerosols that did not contain significant transition metal ions; similarly low uptake coefficients were derived by Thornton and Abbatt (2005). In contrast, measurements by Taketani et al. (2008) suggest higher uptakes of ~0.1 with enhancements observed with increasing relative humidity.

1 The uptake of HO₂ to aqueous aerosols is driven by its high solubility in water owing to its
2 high Henry's Law constant ($H_{\text{HO}_2} = 4.0 \times 10^3 \text{ M atm}^{-1}$ at 298.15 K (Hanson et al., 1992)).
3 Once in the aqueous phase, reaction between dissolved HO₂ and its conjugate base, O₂⁻,
4 occurs rapidly. Thornton et al. (2008) have demonstrated that the solubility and reactivity of
5 HO₂ is temperature and pH dependent and if the well characterised aqueous phase reactions
6 (Sect. 2.3, (R1) – (R5)) alone are representative of the heterogeneous loss processes, only
7 small uptake coefficients would be expected at room temperature, consistent with the work
8 by George et al. (2013) and Thornton and Abbatt (2005). The enhanced uptake coefficients
9 reported by Taketani et al. (2008) suggests that there may be additional competing
10 mechanisms occurring, however.

11
12 Further uncertainties arise in the literature relating to the eventual gas-phase products from
13 these aqueous-phase reactions. The general consensus, until recently, was that these reactions
14 would ultimately produce H₂O₂ (Jacob, 1996), but the significance of the reactions depends
15 critically on whether this is the case or whether, instead, H₂O is produced (Macintyre and
16 Evans, 2011). This is significant as H₂O₂ can photolyse to return odd hydrogen
17 (HO_x=OH+HO₂) to the gas phase, whilst cloud uptake of HO₂ to form H₂O provides a
18 terminal sink for HO_x. Recent work by Mao et al. (2013) postulates that a catalytic
19 mechanism involving the coupling of the transition metal ions Cu(I)/Cu(II) and Fe(II)/Fe(III)
20 may rapidly convert HO₂ to H₂O, rather than H₂O₂ in aqueous aerosols. The concentration
21 and availability of dissolved Fe and Cu in cloud droplets tends to be much lower than in
22 aqueous aerosol (Jacob, 2000) with a large fraction of Cu ions present as organic complexes
23 (Spokes et al., 1996; Nimmo and Fones, 1997) which are far less reactive towards O₂⁻ and
24 HO₂(aq) than the free ions (Jacob, 2000) and so it is uncertain whether the mechanism put
25 forward by Mao et al. (2013) could be extended to heterogeneous processes occurring within
26 cloud droplets.

27 To better understand the role of clouds and heterogeneous processes on the oxidative capacity
28 of the troposphere, coordinated gas-phase measurements of OH and HO₂ within clouds
29 together with aerosol-cloud microphysical measurements are needed. The Hill Cap Cloud
30 Thuringia 2010 (HCCT-2010) campaign which took place in 2010 aimed to characterise the
31 interaction of particulate matter and trace gases in orographic clouds. This paper presents the
32 impact of cloud droplets on measured gas-phase OH and HO₂ and uses these observations to

1 assess the proposed aqueous phase mechanisms and determine the global impact of clouds on
2 the tropospheric oxidising capacity.

3 **2 Experimental**

4 The HCCT-2010 campaign took place at the Thüringer Wald mountain range in central
5 Germany during September and October 2010. The radical measurements were made from
6 the German Weather Service (DWD) and the Federal Environmental Office (UBA) research
7 station located close to the summit of Mt. Schmücke (the highest peak in the mountain range,
8 937 m above sea level, 10°46'8.5" East, 50°39'16.5" North). In October, the UBA station is
9 immersed in cloud for 25 days on average (Herrmann et al., 2005) and, hence, is highly
10 suitable for the study of gas and aerosol interactions with orographic cloud. Two additional
11 experimental sites, approximately 4 km upwind of the summit site at Goldlauter and
12 approximately 3 km downwind of the summit at Gelhberg were also equipped with a number
13 of instruments which enabled the processing of a single air parcel as it passed through a cloud
14 to be assessed by multiphase trajectory models such as SPACCIM (SPectral Aerosol Cloud
15 Chemistry Interaction Model (Wolke et al., 2005); see Sect. 2.3). Further details of the
16 locations may be found in Herrmann et al. (2005).

17 **2.1 Radical measurements**

18 OH and HO₂ measurements were made using the fluorescence assay by gas expansion
19 technique (FAGE). Details of the instrumentation can be found in Whalley et al. (2010). A
20 single FAGE fluorescence cell was used for sequential measurements of OH and HO₂. This
21 was operated from the top of a 22 m high tower to co-locate with cloud measurements and
22 ensure that the measurements were performed in full cloud. The cell was held at 1 Torr using
23 a roots blower backed rotary pump system which was housed in an air-conditioned shipping
24 container at the base of the tower (Fig. 1) and was connected to the cell via 30 m of flexible
25 hosing (5 cm OD). 308 nm tuneable, pulsed laser light was used to electronically excite OH
26 radicals, this was delivered to the cell via a 30 m fibre optic cable (Oz optics) with the laser
27 system (a Nd:YAG pumped Ti:Sapphire, Photonic Industries) housed in the shipping
28 container. Fluorescence was detected by a channel photo multiplier (CPM) (Perkin Elmer)
29 and gated photon counting. Data were acquired every second (photon counts from 5000 laser
30 shots), with a data acquisition cycle consisting of 220 seconds with the laser wavelength
31 tuned to the OH transition (NO was injected after 110 sec to rapidly convert HO₂ to OH, to

1 allow the quantification of HO₂) and 110 sec tuned away from the OH transition to determine
2 the background signal from laser scattered light.

3 The sensitivity of the fluorescence cell for OH and HO₂ was determined twice weekly during
4 the measurement period through calibration using VUV photolysis of H₂O vapour in a
5 turbulent flow of zero air (BOC, BTCA air). Calibrations were performed at relevant H₂O
6 vapour concentrations so as to encompass the ambient H₂O vapour concentrations observed.
7 As such, no correction for quenching of the fluorescence signal due to changing conditions
8 was necessary. The impact of H₂O (v) on the sensitivity of this FAGE cell type (as outlined
9 by Commane et al., (2010)) has been studied by systematically varying the H₂O
10 concentration from 500 ppmV to 10 000 ppmV and only ~ 10 % reduction in sensitivity over
11 this range for both OH and HO₂ was observed. This reduction is entirely explained by the
12 known quenching of fluorescence by H₂O molecules. The lamp flux was determined by N₂O
13 actinometry (see Commane et al. (2010) for further details); this was carried out before and
14 after the campaign and the values agreed within 21%; the average flux was used to determine
15 the sensitivity. The limit of detection (LOD) at a signal to noise ratio of one for one data
16 acquisition cycle was $\sim 6 \times 10^5$ molecule cm⁻³ and $\sim 8.5 \times 10^5$ molecule cm⁻³ for OH and HO₂,
17 respectively.

18 A number of operational modifications (from the standard University of Leeds ground-based
19 operations (Whalley et al., 2010)) were necessary to facilitate measurements of the gas-phase
20 concentrations of the radicals within clouds. As tower measurements were required
21 (schematic of the measurement set-up is provided in Fig. 1), a single, smaller (4.5 cm (ID)
22 diameter stainless steel cylinder) FAGE fluorescence cell, based on the University of Leeds
23 aircraft cell design (Commane et al., 2010) was used for sequential measurements of OH and
24 HO₂. Ambient air was drawn into the cell through a 1 mm diameter pinhole nozzle. The
25 distance between sampling nozzle and radical detection region was 18 cm and NO (10
26 SCCM, BOC, 99.5%) was injected ~8 cm below the nozzle for titration of HO₂ to OH.

27 The fluorescence cell was orientated with the nozzle pointing horizontal to the ground in an
28 attempt to minimise water pooling on the nozzle and being sucked into the cell during cloud
29 events. Occasional droplets were ingested by the cell and resulted in an instantaneous large
30 increase in the laser scattered signal. These spiked increases were discreet and short-lived; the
31 data presented here have been filtered to remove these spikes, which were easy to identify.

1 Tests have been conducted post-campaign to determine the level of HO₂ interference from
 2 RO₂ radicals (Fuchs et al., 2011). Under this particular experimental set-up, an equivalent
 3 amount of ethene-derived RO₂ radicals to HO₂ were found to contribute 46 % to the total
 4 HO₂ signal (Whalley et al., 2013). The FAGE instrument was found not to be sensitive to
 5 CH₃O₂, and other short-chain alkane-derived RO₂ radicals but is sensitive to other alkene and
 6 aromatic derived RO₂ radicals with similar sensitivities to that for ethene-derived RO₂. The
 7 instrument is also sensitive to longer-chain alkane-derived RO₂ radicals (>C₃) albeit to a
 8 smaller extent, as reported by Whalley et al. (2013). For this rural environment, at this time of
 9 year, however, the contribution of alkene and aromatic-derived RO₂ radicals to the total RO₂
 10 budget is expected to be small as the parent VOCs for these particular RO₂ types were at low
 11 concentrations; isoprene concentrations, for example, were on average just 12.6 pptv. As a
 12 consequence of this, the resultant HO₂ interference from RO₂ radicals should also be low.

13 2.2 Model expression and constraints

14 An analytical expression has been used to predict the mean diurnal HO₂ concentrations
 15 throughout the campaign both during cloud events and outside of cloud events. This
 16 expression was originally developed by Carslaw et al. (1999) for modelling OH, HO₂ and
 17 RO₂ radicals in the marine boundary layer and was found to agree with full Master Chemical
 18 Mechanism (MCM) model predictions for OH and HO₂ to within 20% for daytime hours. It
 19 has since been extended further by Smith et al. (2006) to include additional HO₂ sinks, such
 20 as heterogeneous loss (k_{Loss}). The expression, given in Eq. (3), derives from the solution of
 21 simultaneous steady state expressions for OH and CH₃O₂ (Eq. (1) and Eq. (2) below) and
 22 includes any primary sources of HO₂ not coming from radical propagation steps such as
 23 formaldehyde photolysis:

$$24 \quad [OH] = \frac{2f \cdot j(O^1D)[O_3] + [HO_2](k_{HO_2+NO}[NO] + k_{HO_2+O_3}[O_3])}{k_{CO+OH}[CO] + k_{H_2+OH}[H_2] + k_{HCHO+OH}[HCHO] + k_{CH_4+OH}[CH_4] + k_{NO_2+OH}[NO_2] + k_{O_3+OH}[O_3]} \quad (1)$$

$$25 \quad [CH_3O_2] = \frac{k_{CH_4+OH}[CH_4][OH]}{k_{CH_3O_2+HO_2}[HO_2] + k_{CH_3O_2+NO}[NO]} \quad (2)$$

26

$$27 \quad \beta[HO_2]^3 + \gamma[HO_2]^2 + \delta[HO_2] + \varepsilon = 0 \quad (3)$$

28 where

$$\beta = 2k_{T2}(k_{T3}B + k_{T1}A)$$

$$\gamma = 2k_{T3}k_{T2}J_1 + 2k_{T3}k_{P5}[NO]B + 2k_{T2}k_{P4}[CH_4]B + k_T[NO_2]k_{T2}B + 2Ak_{T1}k_{P5}[NO]$$

$$\delta = 2k_{T3}k_{P5}J_1[NO] + 2k_{T2}k_{P4}J_1[CH_4] + k_TJ_1[NO_2]k_{T2} + k_TB[NO_2]k_{P5}[NO] - (J_1 + J_2)Ak_{T2}$$

$$\varepsilon = J_1k_T[NO_2]k_{P5}[NO] - (J_1 + J_2)Ak_{P5}[NO]$$

1 where

$$J_1 = P(OH) = 2f[O_3]j(O^1D)$$

2 (f is the fraction of $O(^1D)$ that reacts with H_2O vapour to form OH , rather than being
3 quenched to $O(^3P)$)

$$J_2 = 2j(HCHO \rightarrow 2HO_2)[HCHO]$$

$$A = k_{CO+OH}[CO] + k_{H_2+OH}[H_2] + k_{HCHO+OH}[HCHO] + k_{CH_4+OH}[CH_4] + k_{NO_2+OH}[NO_2] + k_{O_3+OH}[O_3]$$

$$B = k_{HO_2+NO}[NO] + k_{HO_2+O_3}[O_3] + k_{loss}$$

$$k_T = k_{OH+NO_2}$$

$$k_{T1} = k_{HO_2+HO_2}$$

4 $k_{T2} = k_{HO_2+CH_3O_2}$

5 $k_{T3} = k_{OH+HO_2}$

6 $k_{P4} = k_{CH_4+OH}$

7 $k_{P5} = k_{CH_3O_2+NO}$

8 Limited CO concentration data are available from the summit site during the project, owing
9 to instrumental problems for the first two weeks of measurements. An average CO
10 concentration of 231 ppbv was used in the analytical expression to determine HO_2
11 concentrations although additional model runs at + and - 1σ of this average concentration
12 (297 ppbv and 165 ppbv respectively) were also made to assess the sensitivity of the
13 predicted HO_2 concentration to this constraint. Similarly, only discrete (non-continuous)
14 measurements of HCHO were made during the project; an average value of 479 pptv was

1 used as a model constraint and further model runs at + and - 1σ of this average concentration
2 (818 pptv and 139 pptv respectively) were made.

3 $j(\text{O}^1\text{D})$ was measured from the top of the 22 m tower, alongside the FAGE detection cell,
4 using a $2\text{-}\pi$ filter radiometer (Bohn et al., 2008) which pointed skywards throughout the
5 campaign. The photolysis rates of formaldehyde, $j(\text{HCHO})$, have been calculated using the
6 Tropospheric Ultraviolet and Visible (TUV) radiation model (Madronich and Flocke, 1998).
7 The correlation between TUV calculated $j(\text{HCHO})$ with TUV calculated $j(\text{O}^1\text{D})$ was
8 determined allowing these photolysis rates to be scaled to the measured $j(\text{O}^1\text{D})$ values to
9 account for the presence of clouds. During cloud events, upward radiation will increase, with
10 the magnitude of this increase dependent on the cloud optical depth (COD) and measurement
11 height (Bohn, 2014). The contribution of upward radiation as a function of COD has been
12 estimated using the TUV model using the methodology outlined by Bohn (2014). This
13 estimated increase in upward radiation has been added to the in-cloud photolysis rates
14 presented in Section 3. On average, photolysis rates are enhanced by $\sim 17\%$ during cloud
15 events due to upwelling. A constant value of 1760 ppbv was assumed for CH_4 and a value of
16 508 ppbv was taken for H_2 . O_3 and NO_x measurements were made from the top of the tower
17 using commercial analysers which ran continuously from the 16th September (day 3 of the
18 field project). Details of the ancillary measurements used for comparison and model
19 constraints are provided in Table 1. Further details of many of the measurement techniques
20 can be found in the overview paper from an earlier hill cap cloud experiment, the Field
21 Investigations of Budgets and Conversions of Particle Phase Organics in Tropospheric Cloud
22 Processes (FEBUKA) project (Herrmann et al., 2005).

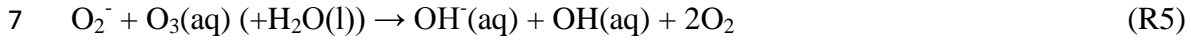
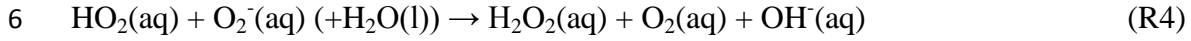
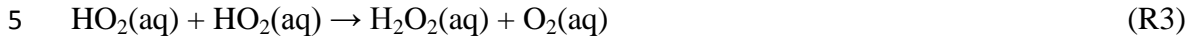
23 Rate coefficients are taken from the most recent recommendations in the Master Chemical
24 Mechanism (MCMv3.2), <http://mcm.leeds.ac.uk/MCM/>.

25 A constant uptake rate for HO_2 (k_{Loss}) of 0.14 s^{-1} to cloud droplets was included during cloud
26 events to reproduce the average HO_2 in-cloud observations. Additional model runs with no
27 uptake during cloud events have also been run for comparison, as have model runs in which
28 the first order loss to droplets was varied to replicate the HO_2 observations as a function of i)
29 cloud droplet surface area and ii) pH (Sect. 3.1).

30

31 **2.3 Aqueous phase chemistry**

1 An outline of the aqueous phase reactions thought to be occurring, and which converts HO₂
 2 to H₂O₂, is given below:



8 The equations used to calculate the theoretical increase in γ_{HO_2} with increasing pH, as
 9 proposed by Thornton et al. (2008), which have been compared with γ_{HO_2} determined in this
 10 work (Sect. 3.1), are given by:

$$11 \frac{1}{\gamma_{\text{HO}_2}} = \frac{1}{\alpha_{\text{HO}_2}} + \frac{3\omega N_A}{8000(H_{\text{eff}}RT)^2 k_{\text{eff}}[\text{HO}_2(\text{g})]r_P} \quad (4)$$

12 where

$$13 H_{\text{eff}} = H_{\text{HO}_2} \left[1 + \frac{K_{\text{eq}}}{[\text{H}^+]} \right] \quad (5)$$

14 and

$$15 k_{\text{eff}} = \frac{k_3 + \left(\frac{K_{\text{eq}}}{[\text{H}^+]_{\text{aq}}} \right) k_4}{\left(1 + \frac{K_{\text{eq}}}{[\text{H}^+]_{\text{aq}}} \right)^2} \quad (6)$$

16 The values used in Eq. (4) – Eq. (6) to calculate γ_{HO_2} are provided in Table 2.

17 **2.4 Trajectory model**

18 In addition to the modelling exercises, outlined in Sect. 2.2 above, an up-to-date chemistry
 19 process model, SPACCIM (SPectral Aerosol Cloud Chemistry Interaction Model (Wolke et
 20 al., 2005)) has been used to simulate the gas phase HO₂ radical concentrations along a
 21 trajectory during the mountain overflow of an air parcel passing an orographic hill cap cloud
 22 to further explore the heterogeneous loss processes occurring during the cloud events
 23 encountered. This model combines complex microphysical and detailed multiphase
 24 chemistry, permitting a detailed description of the chemical processing of gases, deliquesced

1 particles and cloud droplets. SPACCIM incorporates the MCMv3.1-CAPRAMv4.0a
2 mechanism (Master Chemical Mechanism (Saunders et al., 2003) / Chemical Aqueous Phase
3 RAdical Mechanism (Tilgner et al., 2013; Braeuer et al., in preparation)) with 11381 gas
4 phase and 7125 aqueous phase reactions. The MCMv3.1-CAPRAM4.0a mechanism
5 incorporates a detailed description of the inorganic and organic multiphase chemistry
6 including phase transfer in deliquesced particles and cloud droplets based on a time-
7 dependent size-resolved aerosol/cloud spectra. Further details about the SPACCIM model
8 framework and the chemical mechanisms are given elsewhere in the literature (Tilgner et al.,
9 2013; Wolke et al., 2005; Sehili et al., 2005) (and references therein).

10 The measured meteorological data as well as the physical and chemical aerosol and gas phase
11 data at the upwind site in the village of Goldlauter provided the basis for the time-resolved
12 initialisation of the model. In addition, separate initial box model runs with the MCM
13 mechanism were performed to provide a more comprehensive initialisation of the chemical
14 gas phase composition at the simulation start. SPACCIM simulations were performed with an
15 air parcel advected along a predefined orography-following trajectory from the upwind site
16 (Goldlauter) through the hill cap cloud, passing Mt. Schmücke (summit site), to the
17 downwind site (Gehlberg). Parcel simulations were performed every 20 minutes allowing a
18 time-resolved comparison of the predicted and measured HO₂ data at the summit site.

19

20 **2.5 Global chemistry transport model**

21 The GEOS-Chem model version 9.1.3 (www.geoschem.org) has been run to assess the global
22 impact of the uptake of HO₂ by cloud droplets. The model was run at 2x2.5 degree global
23 resolution for two years. The first year was considered a spin-up and has been ignored. The
24 standard model includes uptake of HO₂ onto aerosols (with an uptake coefficient of 0.2), but,
25 the model has been updated in this work to include an uptake of HO₂ onto clouds. This is
26 parameterized as a first order loss onto clouds in a similar way to that onto aerosols following
27 Schwartz (1984) using the temperature dependent parameterization of Thornton et al. (2008)
28 with a cloud pH of 5. The cloud surface area is derived from the cloud liquid water in the
29 each model grid box (provided from the meteorological analyses) and cloud droplet radius is
30 taken to be 6µm over continents and 10µm over oceans. Clouds below 258 K are assumed to
31 be ice and no uptake occurs. The parameterization takes diffusional limitation in the gas
32 phase into account but not in the cloud phase. All simulations use the same cloud liquid water

1 fields, thus the impact of clouds on photolysis, wet deposition and transport is identical in all
2 simulations.

3 **3 Results and Discussion**

4 Near continuous OH and HO₂ measurements were made at the Mt. Schmücke site from 13th
5 September to 19th October 2010, during which 35 separate orographic cloud events were
6 encountered which lasted as little as 24 min to more than 2 days in duration. Fig. 2 shows the
7 time-series of OH, HO₂, $j(\text{O}^1\text{D})$, NO, O₃ and liquid water content. OH concentrations were
8 close to or below the limit of detection (LOD) of the instrument for much of the measurement
9 period. A clear diurnal signal was only observable when several days of data were averaged
10 together outside of cloud events (Fig. 3). The peak OH concentration was observed at midday
11 at $\sim 1 \times 10^6$ molecule cm⁻³. No clear OH diurnal profile was observed during cloud events.
12 HO₂ concentrations were variable depending on whether the site was in cloud or not. The
13 average diurnal peak concentration of HO₂ was $\sim 4 \times 10^7$ molecule cm⁻³ outside of cloud
14 events (Fig. 3). A diurnal profile of HO₂ was also observed when sampling within clouds
15 with peak concentrations reduced by approximately 90% on average. The measured rate of
16 ozone photolysis, $j(\text{O}^1\text{D})$, varied with time of day and cloud thickness. Daily peak photolysis
17 rates were $8.8 \times 10^{-6} \text{ s}^{-1}$ and $4.1 \times 10^{-6} \text{ s}^{-1}$ outside and within clouds, respectively. Clouds thus
18 reduced photolysis rates by $\sim 60\%$.

19 Fig. 4 shows the dependence of measured HO₂ concentration on cloud droplet surface area
20 for all daytime cloud events. The observed HO₂ concentration has been divided by the
21 observed $j(\text{O}^1\text{D})$ to remove the impact of the changing photolysis rates within the cloud. This
22 ratio has then been normalized to 1 when the droplet surface area was zero and plotted
23 against the cloud droplet surface area. The decrease in the ratio with increasing droplet
24 surface area suggests that in addition to the reduction in HO₂ caused by a reduction in the
25 photolysis rates within clouds, there is a further loss process of HO₂ that increases with cloud
26 droplet surface area. A similar decrease in the ratio is also observed with increasing liquid
27 water (not shown). From these observations it becomes apparent that a heterogeneous process
28 must be occurring in the presence of clouds.

29 An insight into the mechanism by which HO₂ is lost to clouds is demonstrated by the
30 dependence of the measured HO₂ concentration as a function of cloud water pH (Fig. 5a).
31 Throughout the project the pH of the cloud water was recorded every hour and ranged from

1 3.4 to 5.3. The lowest in-cloud HO₂ occurred in clouds with the highest cloud water pH
2 suggesting that the solubility of HO₂ was enhanced at higher pH as might be expected given
3 that HO₂ is a weak acid.

4 **3.1 Determining the uptake coefficient for HO₂ to cloud droplets**

5 The analytical expression derived by Carslaw et al.(1999), and given in Eq. (3), has been
6 used to estimate HO₂ concentrations both in and out of cloud events (Fig. 6). The expression
7 represents reasonably well the campaign mean diurnal observation of HO₂ outside of the
8 cloud events during the daytime (red dashed line and shading). During cloud events,
9 however, the model (black dashed line and shading) over-estimates the observed (grey line)
10 HO₂ throughout the day. The inclusion of a first order loss process ($k_{Loss}=0.14\text{ s}^{-1}$) in the
11 analytical expression is able to bring the observations and calculation into better agreement
12 on average. The cloud droplet surface area was variable during the different cloud events
13 encountered ($1.2\pm 0.4\times 10^3\text{ cm}^2\text{ m}^{-3}$) although no diurnal trend in this parameter was evident.
14 A clear anti-correlation between the observed HO₂ concentration and droplet surface area was
15 observed and this correlation could only be reproduced by the analytical expression by
16 increasing k_{Loss} in the model from $2.0\times 10^{-2}\text{ s}^{-1}$ to $3.5\times 10^{-1}\text{ s}^{-1}$ as the surface area increased
17 from $1.2\times 10^2\text{ cm}^2\text{ m}^{-3}$ to $1.5\times 10^3\text{ cm}^2\text{ m}^{-3}$ (Fig. 7).

18 This first order loss rate can be converted into an uptake coefficient (γ_{HO_2}) using Eq. (7)
19 (Schwartz, 1984). Using campaign mean values for cloud surface area (A) of $1.2\times 10^3\text{ cm}^2\text{ m}^{-3}$
20 ³, droplet radius (r_p) of 6 μm , gas phase diffusion constant for HO₂ (D_g) of $0.25\text{ cm}^2\text{ s}^{-1}$, and
21 molecular speed of HO₂ (ω) of 64000 cm s^{-1} gives an uptake coefficient of 0.01; the uptake
22 coefficient as a function of cloud droplet surface area is presented in the upper panel of figure
23 7.

$$24 \quad k_{loss} = \left(\frac{r_p}{D_g} + \frac{4}{\gamma_{HO_2}\omega} \right)^{-1} A \quad (7)$$

25 These derived uptake coefficients are in good agreement with laboratory studies (Abbatt et
26 al., 2012), including recent measurements in our laboratory, which ranged between 0.003 –
27 0.02, for heterogeneous loss of HO₂ on aqueous (NH₄)₂SO₄, NaCl and NH₄NO₃ sub-micron
28 aerosols (George et al., 2013). This methodology provides, for the first time, a direct field
29 assessment of the heterogeneous rate of loss of HO₂.

1 Repeating this analysis but splitting the observations by cloud pH leads to values of
2 γ_{HO_2} ranging from 1.65×10^{-3} at a pH of 3.7 to 8.84×10^{-2} at a pH of 5.2 (Fig. 5b). These values
3 are in good agreement with those calculated by Thornton et al. (2008) suggesting that the
4 Thornton mechanism (which is based entirely on the known aqueous phase chemistry) is in
5 play in real clouds and that it can be used to estimate the heterogeneous loss of HO_2 to cloud
6 surfaces in the troposphere.

7 SPACCIM simulations (Wolke et al., 2005) have also been carried out, focussing on one
8 particular cloud event which fulfilled the required meteorological and connected flow
9 conditions for the cloud passage experiment (additional simulations relating to the other
10 cloud events encountered during HCCT will be presented in future publications). The
11 modelled and measured HO_2 concentrations at Mt. Schmücke during the cloud event,
12 FCE1.1, are presented in Fig. 8. Comparisons between modelled and measured
13 concentrations demonstrate the simulated HO_2 concentrations are in a similar range as the
14 measurements. The mean simulated HO_2 concentrations of 3.1×10^6 molecule cm^{-3} for
15 FCE1.1 are a factor of 1.4 greater than the HO_2 measurements which were, on average
16 2.2×10^6 molecule cm^{-3} during this particular cloud event. A further trajectory model
17 simulation has been run and compared to measured HO_2 concentrations at Mt. Schmücke
18 during a non-cloud event, NCE0.8, also. Fig. 9 reveals that the model is able to reproduce the
19 modelled HO_2 concentrations well and tracks the temporal concentration profile throughout
20 this event. The mean predicted HO_2 concentration is just 24% smaller than the measurements.

21 The agreement between the trajectory modelled and measured in-cloud HO_2 values confirms
22 the significant reductions of radicals within clouds predicted by complex multiphase box
23 models in the past (Lelieveld and Crutzen, 1990; Tilgner et al., 2005; Tilgner et al., 2013) and
24 supports the findings presented above. Importantly, the results imply that the phase transfer
25 data for HO_2 used within SPACCIM simulations, e.g. the applied mass accommodation
26 coefficient ($\alpha_{HO_2} = 10^{-2}$), are appropriate to reproduce the reduced HO_2 concentrations for in-
27 cloud conditions. These applied parameters control the uptake fluxes towards the aqueous
28 phase and, ultimately, the aqueous phase HO_x levels. Confidence in the values assumed for
29 these parameters is essential to model in-cloud oxidation within the aqueous phase
30 accurately, with the multiphase chemistry of other important chemical subsystems, such as
31 the S(IV) to S(VI) conversion, the redox-cycling of transition metal ions and the processing
32 of organic compounds all heavily dependent upon the values taken.

1 **3.2 Global impact of the uptake of HO₂ onto cloud droplets**

2 The GEOS-Chem Chemistry Transport Model (www.geos-chem.org) has been used to assess
3 the impact of the uptake of HO₂ onto cloud droplets on the global oxidizing capacity using
4 the, now field-validated, mechanism of Thornton et al. (2008). To investigate both the impact
5 of the uptake and whether H₂O₂ is produced three simulations are run, i) with no cloud uptake
6 of HO₂, ii) with cloud uptake (assumed pH of 5) of HO₂ using the Thornton mechanism to
7 produce H₂O₂, and iii) with cloud uptake (assumed pH of 5) of HO₂ to produce H₂O. All
8 simulations include HO₂ uptake onto aerosol with γ_{HO_2} of 0.2, which is the standard value
9 used in GEOS-Chem (Martin et al., 2003; Macintyre and Evans, 2011).

10 Fig. 10 shows the annual fractional change in surface HO₂, OH, H₂O₂ and O₃ concentrations
11 with cloud uptake switched on, and with either H₂O₂ being produced or not. Column changes
12 are shown in Fig. 11. Both with and without H₂O₂ production, the impact is most evident in
13 areas with long HO₂ lifetimes, i.e. regions with low NO_x and low HO₂ concentrations, and
14 with significant cloud water densities (see Figure 12). These are concentrated in the extra-
15 tropics with up to 25% and 10% reduction in surface and column concentrations respectively.
16 The impact on the H₂O₂ concentration depends critically on whether H₂O₂ is produced or not
17 within clouds. In the extra-tropics there are up to 30% increases in surface H₂O₂ if it is
18 produced with a similar reduction if it is not. The impact on surface extra-tropical oxidizing
19 capacity (OH) are of the order 10-20% for both cases, but changes to the column values are
20 only significant in the case where H₂O₂ is not produced. Changes in O₃ concentration are
21 surprisingly small in both simulations. This reflects both the anti-correlation between NO
22 concentrations and HO₂ lifetimes, and the low cloud water densities over the polluted
23 continental regions. The largest fractional changes in HO₂ concentration occur in regions
24 which are not producing O₃. The change in the lifetime due to the HO₂ uptake onto clouds
25 thus has little impact on O₃ production. The large surface impact of the cloud uptake
26 primarily reflects uptake of HO₂ by clouds at the surface (see figure 12a) rather than a
27 transported impact of cloud processes from aloft downwards. The small impact on O₃ is
28 consistent with results of Liang and Jacob, (1997). These simulations make a variety of
29 approximations (see Sect. 2.5) but they indicate that the uptake of HO₂ onto clouds at the
30 rates observed in this field campaign may offer a substantial perturbation to the oxidizing
31 capacity (OH and H₂O₂) of the atmosphere, especially in the extra-tropics, but seems to have
32 a very small impact on O₃ concentrations.

1 **4 Conclusions**

2 We have shown here experimentally for the first time that the uptake of HO₂ onto clouds can
3 have a significant impact on the composition of the atmosphere in a way consistent with
4 theoretical predictions. It seems likely, however, that chemistry occurring within clouds will
5 have other currently unknown impacts on the composition of the atmosphere. Global and
6 regional models need to be developed further to investigate these impacts with predictive pH
7 an especially important development. The impact of these processes may also change in the
8 future with climate induced impacts on the hydrological cycle. Further laboratory, field
9 studies and modelling are required to help resolve these remaining complex questions.

10 **Acknowledgements**

11 The authors would like to thank Dr. Trevor Ingham, John Spence and Matthew Broadbent for
12 help with the development of the FAGE instrument to facilitate tower measurements. HCCT-
13 2010 was partially funded by the German Research Foundation (DFG), grant He 3086/15-1.
14 SM participation was funded by DFG, grant ME-3534/1-2. LW, DS, IG, ME and DH are
15 grateful to the Natural Environment Research Council for funding.

16

17 **References**

- 18 Abbatt, J. P. D., Lee, A. K. Y., and Thornton, J. A.: Quantifying trace gas uptake to
19 tropospheric aerosol: recent advances and remaining challenges, *Chemical Society Reviews*,
20 41, 6555-6581, Doi 10.1039/C2cs35052a, 2012.
- 21 Bielski, B. H. J., Cabelli, D. E., Arudi, R. L., and Ross, A. B.: Reactivity of HO₂/O₂ radicals
22 in aqueous solution, *Journal of Physical and Chemical Reference Data*, 14, 1041-1100, Doi
23 10.1063/1.555739, 1985.
- 24 Bohn, B., Corlett, G. K., Gillmann, M., Sanghavi, S., Stange, G., Tensing, E., Vrekoussis,
25 M., Bloss, W. J., Clapp, L. J., Kortner, M., Dorn, H. P., Monks, P. S., Platt, U., Plass-Dulmer,
26 C., Mihalopoulos, N., Heard, D. E., Clemitshaw, K. C., Meixner, F. X., Prevot, A. S. H., and
27 Schmitt, R.: Photolysis frequency measurement techniques: results of a comparison within
28 the ACCENT project, *Atmos. Chem. Phys.*, 8, 5373-5391, 2008.
- 29 Bohn, B.: Interactive comment, *Atmos Chem Phys Discuss*, 14, C7390-C7394, 2014.

1 Braeuer, P., Mouchel-Vallon, C., Tilgner, A., Mutzel, A., Böge, O., Rodigast, M., Poulain, L,
2 van Pinxteren, D., Wolke, R., Aumont, B., and Herrmann, H.: Development of a protocol
3 designed for the self-generation of explicit aqueous phase oxidation schemes of organic
4 compounds, in preparation for Atmos Chem Phys Discuss.

5 Carslaw, N., Jacobs, P. J., and Pilling, M. J.: Modeling OH, HO₂, and RO₂ radicals in the
6 marine boundary layer 2. Mechanism reduction and uncertainty analysis, Journal of
7 Geophysical Research-Atmospheres, 104, 30257-30273, Doi 10.1029/1999jd900782, 1999.

8 Commane, R., Floquet, C. F. A., Ingham, T., Stone, D., Evans, M. J., and Heard, D. E.:
9 Observations of OH and HO₂ radicals over West Africa, Atmos Chem Phys, 10, 8783-8801,
10 DOI 10.5194/acp-10-8783-2010, 2010.

11 Emmerson, K. M., Carslaw, N., Carslaw, D. C., Lee, J. D., McFiggans, G., Bloss, W. J.,
12 Gravestock, T., Heard, D. E., Hopkins, J., Ingham, T., Pilling, M. J., Smith, S. C., Jacob, M.,
13 and Monks, P. S.: Free radical modelling studies during the UK TORCH campaign in
14 summer 2003, Atmos Chem Phys, 7, 167-181, 2007.

15 Fuchs, H., Bohn, B., Hofzumahaus, A., Holland, F., Lu, K. D., Nehr, S., Rohrer, F., and
16 Wahner, A.: Detection of HO₂ by laser-induced fluorescence: Calibration and interferences
17 from RO₂ radicals, Atmospheric Measurement Techniques, 4, 1209-1225, DOI 10.5194/amt-
18 4-1209-2011, 2011.

19 George, I. J., Matthews, P. S. J., Whalley, L. K., Brooks, B., Goddard, A., Romero, M. T. B.,
20 and Heard, D. E.: Measurements of uptake coefficients for heterogeneous loss of HO₂ onto
21 submicron inorganic salt aerosols, Physical Chemistry Chemical Physics, 15, 12859-12845,
22 2013.

23 Haggerstone, A. L., Carpenter, L. J., Carslaw, N., and McFiggans, G.: Improved model
24 predictions of HO₂ with gas to particle mass transfer rates calculated using aerosol number
25 size distributions, Journal of Geophysical Research-Atmospheres, 110, Artn D04304 Doi
26 10.1029/2004jd005282, 2005.

27 Hanson, D. R., Burkholder, J. B., Howard, C. J., and Ravishankara, A. R.: Measurement of
28 OH and HO₂ Radical Uptake Coefficients on Water and Sulfuric-Acid Surfaces, Journal of
29 Physical Chemistry, 96, 4979-4985, Doi 10.1021/J100191a046, 1992.

30 Herrmann, H., Wolke, R., Muller, K., Bruggemann, E., Gnauk, T., Barzagli, P., Mertes, S.,
31 Lehmann, K., Massling, A., Birmili, W., Wiedensohler, A., Wierprecht, W., Acker, K.,
32 Jaeschke, W., Kramberger, H., Svrčina, B., Bachmann, K., Collett, J. L., Galgon, D.,
33 Schwirn, K., Nowak, A., van Pinxteren, D., Plewka, A., Chemnitz, R., Rud, C., Hofmann,
34 D., Tilgner, A., Diehl, K., Heinold, B., Hinneburg, D., Knoth, O., Sehili, A. M., Simmel, M.,

1 Wurzler, S., Majdik, Z., Mauersberger, G., and Muller, F.: FEBUKO and MODMEP: Field
2 measurements and modelling of aerosol and cloud multiphase processes, *Atmos Environ*, 39,
3 4169-4183, DOI 10.1016/j.atmosenv.2005.02.004, 2005.

4 Huijnen, V., Williams, J. E., and Flemming, J.: Modeling global impacts of heterogeneous
5 loss of HO₂ on cloud droplets, ice particles and aerosols, *Atmospheric Chemistry and Physics*
6 *Discussions*, 14, 8575-8632, 2014.

7 Jacob, D. J.: Chemistry of OH in remote clouds and its role in the production of formic acid
8 and peroxymonosulfate, *Journal of Geophysical Research-Atmospheres*, D9, 9807-9826,
9 1986.

10 Jacob, D. J.: Heterogeneous chemistry and tropospheric ozone, *Atmos Environ*, 34, 2131-
11 2159, Doi 10.1016/S1352-2310(99)00462-8, 2000.

12 Lelieveld, J., and Crutzen, P. J.: Influences of cloud photochemical processes on tropospheric
13 ozone, *Nature*, 343, 227-233, Doi 10.1038/343227a0, 1990.

14 Liang, J., and Jacob, D. J.: Effect of aqueous phase cloud chemistry on tropospheric ozone,
15 *Journal of Geophysical Research-Atmospheres*, 102, D5, 5993-6001, 1997.

16 Macintyre, H. L., and Evans, M. J.: Parameterisation and impact of aerosol uptake of HO₂ on
17 a global tropospheric model, *Atmos Chem Phys*, 11, 10965-10974, DOI 10.5194/acp-11-
18 10965-2011, 2011.

19 Madronich, S., and Flocke, S.: The role of solar radiation in atmospheric chemistry,
20 *Handbook of Environmental Chemistry*, edited by: Boule, P., Springer, New York, pp. 1-26
21 pp., 1998.

22 Mao, J., Fan, S., Jacob, D. J., and Travis, K. R.: Radical loss in the atmosphere from Cu-Fe
23 redox coupling in aerosols, *Atmos Chem Phys*, 13, 509-519, DOI 10.5194/acp-13-509-2013,
24 2013.

25 Martin, R. V., Jacob, D. J., Yantosca, R. M., Chin, M., and Ginoux, P.: Global and regional
26 decreases in tropospheric oxidants from photochemical effects of aerosols, *Journal of*
27 *Geophysical Research-Atmospheres*, 108, D3, 4097, doi:10.1029/2002JD0022622, 2003.

28 Mauldin, R. L., Madronich, S., Flocke, S. J., Eisele, F. L., Frost, G. J., and Prevot, A. S. H.:
29 New insights on OH: Measurements around and in clouds, *Geophysical Research Letters*, 24,
30 3033-3036, 10.1029/97gl02983, 1997.

31 Mauldin, R. L., Frost, G. J., Chen, G., Tanner, D. J., Prevot, A. S. H., Davis, D. D., and
32 Eisele, F. L.: OH measurements during the first Aerosol Characterization Experiment (ACE
33 1): Observations and model comparisons, *Journal of Geophysical Research-Atmospheres*,
34 103, 16713-16729, Doi 10.1029/98jd00882, 1998.

1 Nimmo, M., and Fones, G. R.: The potential pool of Co, Ni, Cu, Pb and Cd organic
2 complexing ligands in coastal and urban rain waters, *Atmos Environ*, 31, 693-702, Doi
3 10.1016/S1352-2310(96)00243-9, 1997.

4 Olson, J. R., Crawford, J. H., Chen, G., Fried, A., Evans, M. J., Jordan, C. E., Sandholm, S.
5 T., Davis, D. D., Anderson, B. E., Avery, M. A., Barrick, J. D., Blake, D. R., Brune, W. H.,
6 Eisele, F. L., Flocke, F., Harder, H., Jacob, D. J., Kondo, Y., Lefer, B. L., Martinez, M.,
7 Mauldin, R. L., Sachse, G. W., Shetter, R. E., Singh, H. B., Talbot, R. W., and Tan, D.:
8 Testing fast photochemical theory during TRACE-P based on measurements of OH, HO₂,
9 and CH₂O, *Journal of Geophysical Research-Atmospheres*, 109, Artn D15s10 Doi
10 10.1029/2003jd004278, 2004.

11 Saunders, S. M., Jenkin, M. E., Derwent, R. G., and Pilling, M. J.: Protocol for the
12 development of the Master Chemical Mechanism, MCM v3 (Part A): tropospheric
13 degradation of non-aromatic volatile organic compounds, *Atmos Chem Phys*, 3, 161-180,
14 2003.

15 Schwartz, S. E.: Gas-phase and aqueous-phase chemistry of HO₂ in liquid water clouds,
16 *Journal of Geophysical Research-Atmospheres*, 89, 1589-1598, Doi
17 10.1029/Jd089id07p11589, 1984.

18 Sehili, A. M., Wolke, R., Knoth, O., Simmel, M., Tilgner, A., and Herrmann, H.: Comparison
19 of different model approaches for the simulation of multiphase processes, *Atmos Environ*, 39,
20 4403-4417, DOI 10.1016/j.atmosenv.2005.02.039, 2005.

21 Smith, S. C., Lee, J. D., Bloss, W. J., Johnson, G. P., Ingham, T., and Heard, D. E.:
22 Concentrations of OH and HO₂ radicals during NAMBLEX: measurements and steady state
23 analysis, *Atmos Chem Phys*, 6, 1435-1453, 2006.

24 Sommariva, R., Haggerstone, A. L., Carpenter, L. J., Carslaw, N., Creasey, D. J., Heard, D.
25 E., Lee, J. D., Lewis, A. C., Pilling, M. J., and Zador, J.: OH and HO₂ chemistry in clean
26 marine air during SOAPEX-2, *Atmos Chem Phys*, 4, 839-856, 2004.

27 Spokes, L. J., Campos, M. L. A. M., and Jickells, T. D.: The role of organic matter in
28 controlling copper speciation in precipitation, *Atmos Environ*, 30, 3959-3966, Doi
29 10.1016/1352-2310(96)00125-2, 1996.

30 Taketani, F., Kanaya, Y., and Akimoto, H.: Kinetics of heterogeneous reactions of HO₂
31 radical at ambient concentration levels with (NH₄)₂SO₄ and NaCl aerosol particles, *Journal*
32 *of Physical Chemistry A*, 112, 2370-2377, Doi 10.1021/Jp0769936, 2008.

1 Thornton, J., and Abbatt, J. P. D.: Measurements of HO₂ uptake to aqueous aerosol: Mass
2 accommodation coefficients and net reactive loss, *Journal of Geophysical Research-*
3 *Atmospheres*, 110, Artn D08309 Doi 10.1029/2004jd005402, 2005.

4 Thornton, J. A., Jaegle, L., and McNeill, V. F.: Assessing known pathways for HO₂ loss in
5 aqueous atmospheric aerosols: Regional and global impacts on tropospheric oxidants, *Journal*
6 *of Geophysical Research-Atmospheres*, 113, Artn D05303 Doi 10.1029/2007jd009236, 2008.

7 Tilgner, A., Majdik, Z., Sehili, A. M., Simmel, M., Wolke, R., and Herrmann, H.:
8 SPACCIM: Simulations of the multiphase chemistry occurring in the FEBUKO hill cap cloud
9 experiments, *Atmos Environ*, 39, 4389-4401, DOI 10.1016/j.atmosenv.2005.02.028, 2005.

10 Tilgner, A., Brauer, P., Wolke, R., and Herrmann, H.: Modelling multiphase chemistry in
11 deliquescent aerosols and clouds using CAPRAM3.0i, *Journal of Atmospheric Chemistry*, 70,
12 221-256, DOI 10.1007/s10874-013-9267-4, 2013.

13 Whalley, L. K., Furneaux, K. L., Goddard, A., Lee, J. D., Mahajan, A., Oetjen, H., Read, K.
14 A., Kaaden, N., Carpenter, L. J., Lewis, A. C., Plane, J. M. C., Saltzman, E. S.,
15 Wiedensohler, A., and Heard, D. E.: The chemistry of OH and HO₂ radicals in the boundary
16 layer over the tropical Atlantic ocean, *Atmos Chem Phys*, 10, 1555-1576, DOI 10.5194/acp-
17 10-1555-2010, 2010.

18 Whalley, L. K., Blitz, M. A., Desservettaz, M., Seakins, P. W., and Heard, D. E.: Reporting
19 the sensitivity of laser-induced fluorescence instruments used for HO₂ detection to an
20 interference from RO₂ radicals and introducing a novel approach that enables HO₂ and
21 certain RO₂ types to be selectively measured, *Atmospheric Measurement Techniques*, 6,
22 3425–3440, 2013.

23 Wolke, R., Sehili, A. M., Simmel, M., Knoth, O., Tilgner, A., and Herrmann, H.: SPACCIM:
24 A parcel model with detailed microphysics and complex multiphase chemistry, *Atmos*
25 *Environ*, 39, 4375-4388, DOI 10.1016/j.atmosenv.2005.02.038, 2005.

26

27

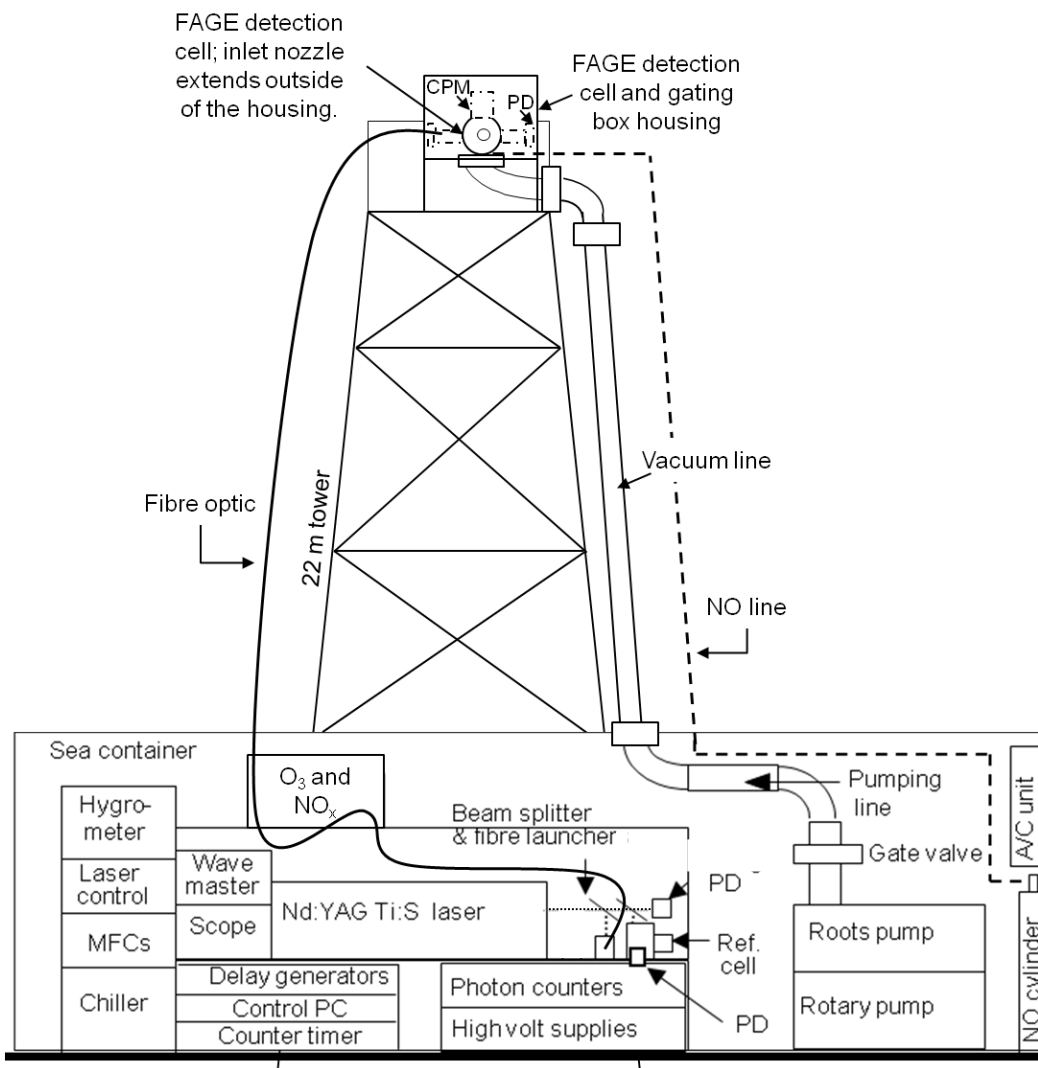
28

- 1 Table 1. Details of ancillary measurements used for comparison with radical observations and
 2 cubic model constraints.

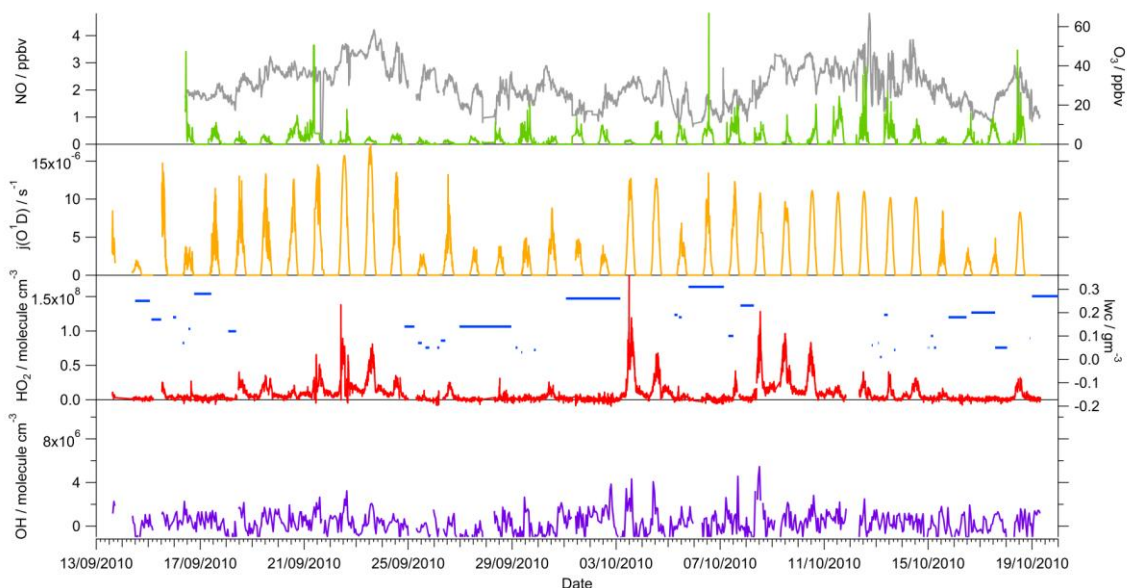
Measurement	Instrument
Liquid Water Content	Gerber particle volume monitor
Particle Surface Area (drops)	Gerber particle volume monitor
Effective Drop Radius	Gerber particle volume monitor
Temperature	Automatic weather station
Relative Humidity	Automatic weather station
$j(O^1D)$	Filter Radiometer
Cloud droplet pH	Mettler 405-60 88TE-S7/120
NO_x	Chemiluminescence detector
O_3	TEI 42c, UV absorption
CO	Thermo Electron CO analyser
HCHO	2,4-dinitrophenylhydrazine (DNPH) cartridge samples

- 3
 4 Table 2. The values used for the calculation of the theoretical uptake coefficient, black
 5 triangles, Fig. 5b, as a function of pH; values given at a pH = 5 here.

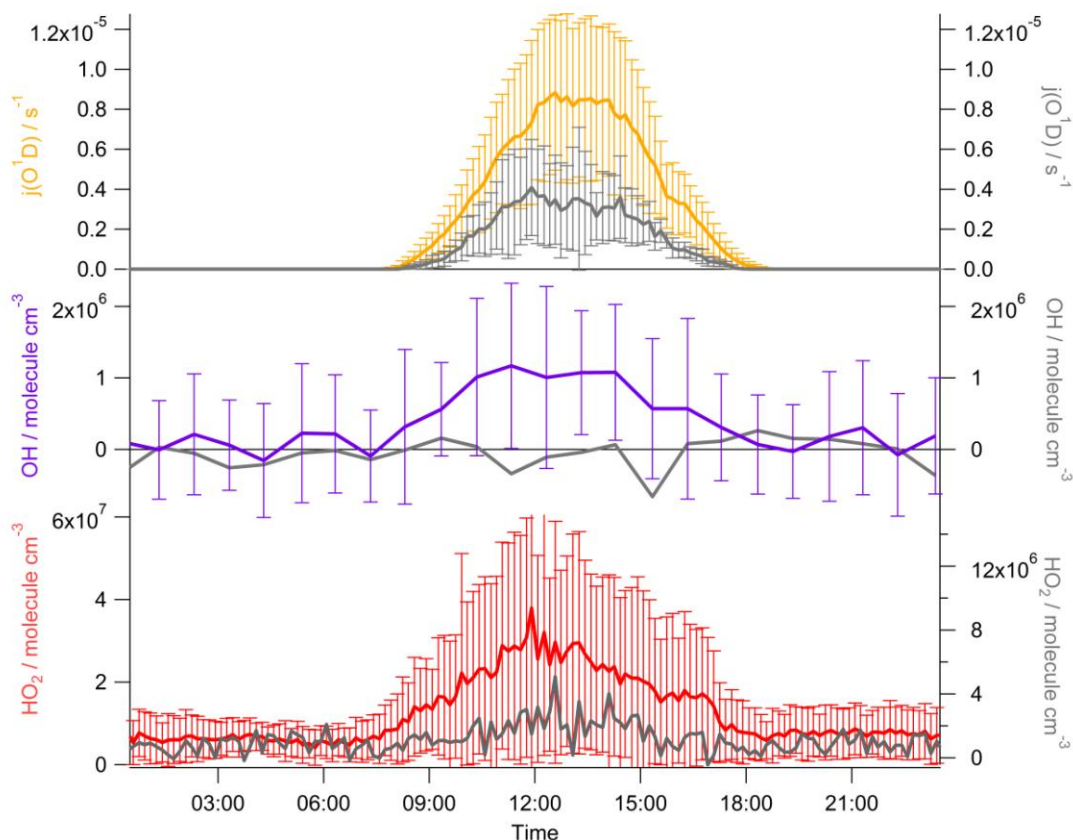
Parameter	Value	Comments
T (Temperature)	279 K	Mean HCCT-2010 temperature
H_{HO_2} (Henry's law constant)	$1.72 \times 10^4 \text{ M atm}^{-1}$	At 279 K
H_{eff} (Effective Henry's law constant)	8.8×10^4	At 279 K, pH = 5
K_{eq} (Equilibrium constant associated with R2)	$4.2 \times 10^{-5} \text{ M}$	At 279 K
k_3 (Rate constant for reaction R3)	$8.6 \times 10^5 \text{ M}^{-1} \text{ s}^{-1}$	Bielski et al.(1985)
k_4 (Rate constant for reaction R4)	$1.0 \times 10^8 \text{ M}^{-1} \text{ s}^{-1}$	Bielski et al.(1985)
k_{eff} (effective second order rate constant)	$1.65 \times 10^7 \text{ M}^{-1} \text{ s}^{-1}$	At 279 K, pH = 5
α_{HO_2} (accommodation coefficient)	1	
ω (mean molecule speed of HO_2)	64000 cms^{-1}	At 279 K
N_A (Avogadro's number)	$6.02 \times 10^{23} \text{ mol}^{-1}$	
R (Universal gas constant)	$0.082057 \text{ atm L mol}^{-1} \text{ K}^{-1}$	
$[HO_2]$	$2 \times 10^7 \text{ molecule cm}^{-3}$	
r_p (particle radius)	6 μm	Mean cloud droplet radius



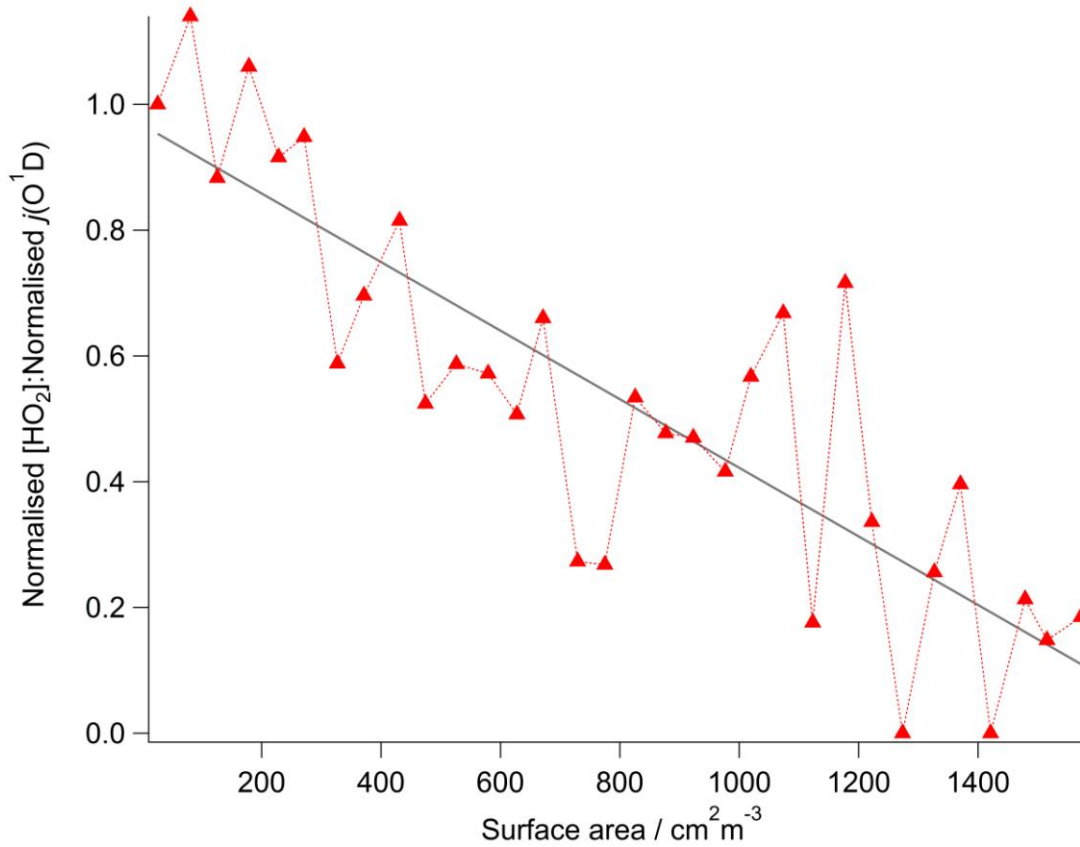
1
 2 Figure 1. Schematic of the FAGE instrument setup during the HCCT-2010 campaign. 'PD'
 3 refers to photodiode, used to normalise the observed HO₂ signal to laser power.



1 Figure 2. Time-series showing the average liquid water content during each cloud episode
 2 (blue, horizontal lines), [OH] (purple), [HO₂] (red), j(O¹D) (orange), NO (green) and O₃
 3 (grey). All data are the average concentrations determined for each FAGE data acquisition
 4 cycle apart from OH concentrations which are hourly.



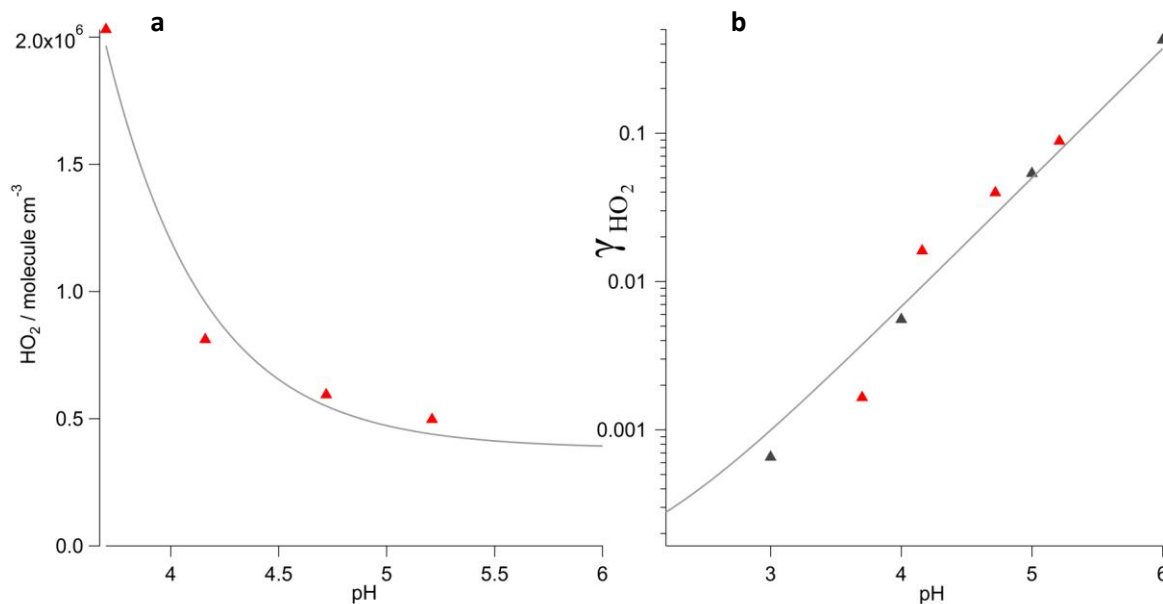
5
 6 Figure 3. Average diurnal profiles of $j(\text{O}^1\text{D})$, OH, HO₂ in cloud (grey) and out of cloud
 7 (coloured). The error bars represent the 1σ variability of the averaged data; only the
 8 variability in the out of cloud radical data is shown for clarity. Each data point represents 10
 9 minute averaged data apart from the OH, for which the hourly averaged data are given.



1

2 Figure 4. The dependence of the measured HO₂ concentration as a function of cloud droplet
 3 surface area. To remove the influence of changing photolysis rates the measured HO₂
 4 concentrations have been divided by the correspondingly observed rate of photolysis of ozone
 5 ($j(\text{O}^1\text{D})$). This ratio has then been normalized to give a value of 1 when the droplet surface
 6 area was zero. The systematic decrease in this normalised ratio with increasing droplet
 7 surface area suggests that in addition to the reduction in HO₂ caused by a reduction in the
 8 photolysis rates within clouds, there is a further loss process that increases with cloud droplet
 9 surface area. The ratio decreases linearly with increasing droplet surface area up to 1500
 10 cm²m⁻³ with the line of best fit being $\text{Ratio} = 1 - 5 \times 10^{-4} \times \text{SA}$.

11



1

2 Figure 5a. Dependence of the HO₂ concentration observed in cloud as a function of cloud pH.

3 All in-cloud HO₂ data were averaged into corresponding pH bins (0.6 pH units). The [HO₂]

4 decreases exponentially with increasing pH with the line of best fit ($[HO_2] = 3.8 \times 10^5 +$

5 $5.5 \times 10^9 \exp^{-2.2pH}$) displayed by the grey line. Figure 5b. The cloud uptake coefficient

6 estimated by optimizing the HO₂ concentration calculated from the analytic expression of

7 Carlsaw et al. (1999) compared to the observed HO₂ concentration as a function of pH (red

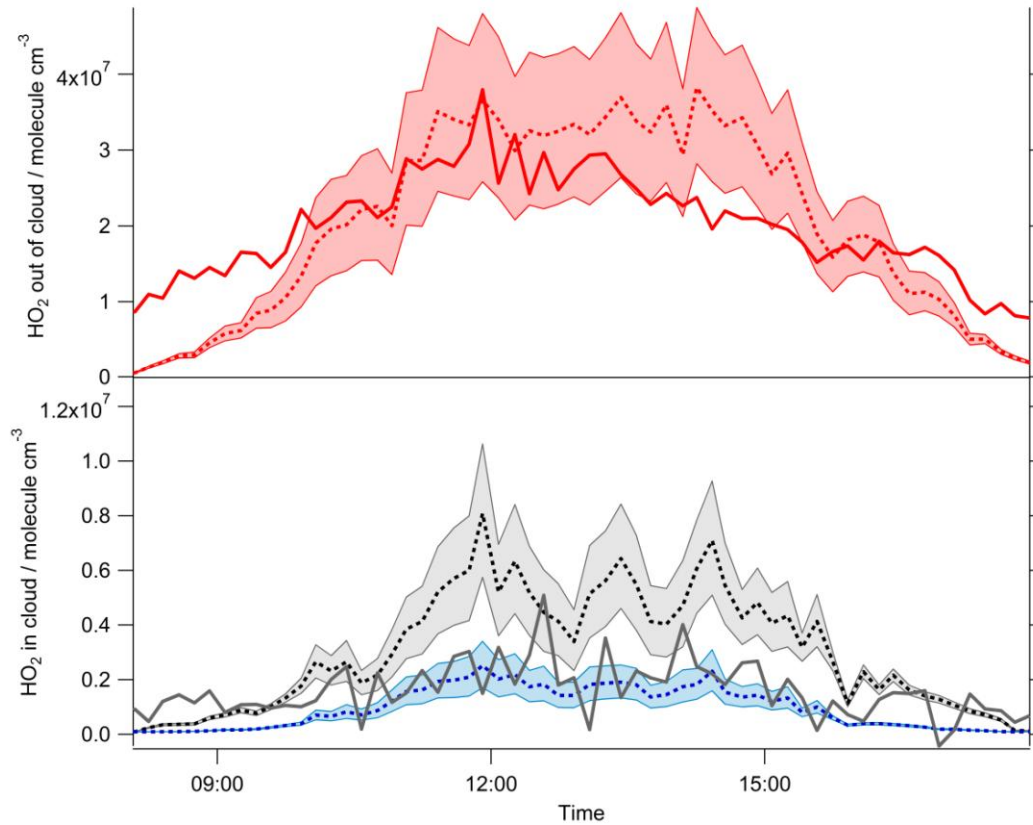
8 triangles). The theoretical expression derived by Thornton et al. (2008) (Eq. (4)) using

9 parameters provided in Table 2 is shown as the black triangles with the grey line being a best-

10 fit line for these data ($\gamma_{HO_2} = 2.15 \times 10^{-6} \exp^{2.01pH}$).

11

12

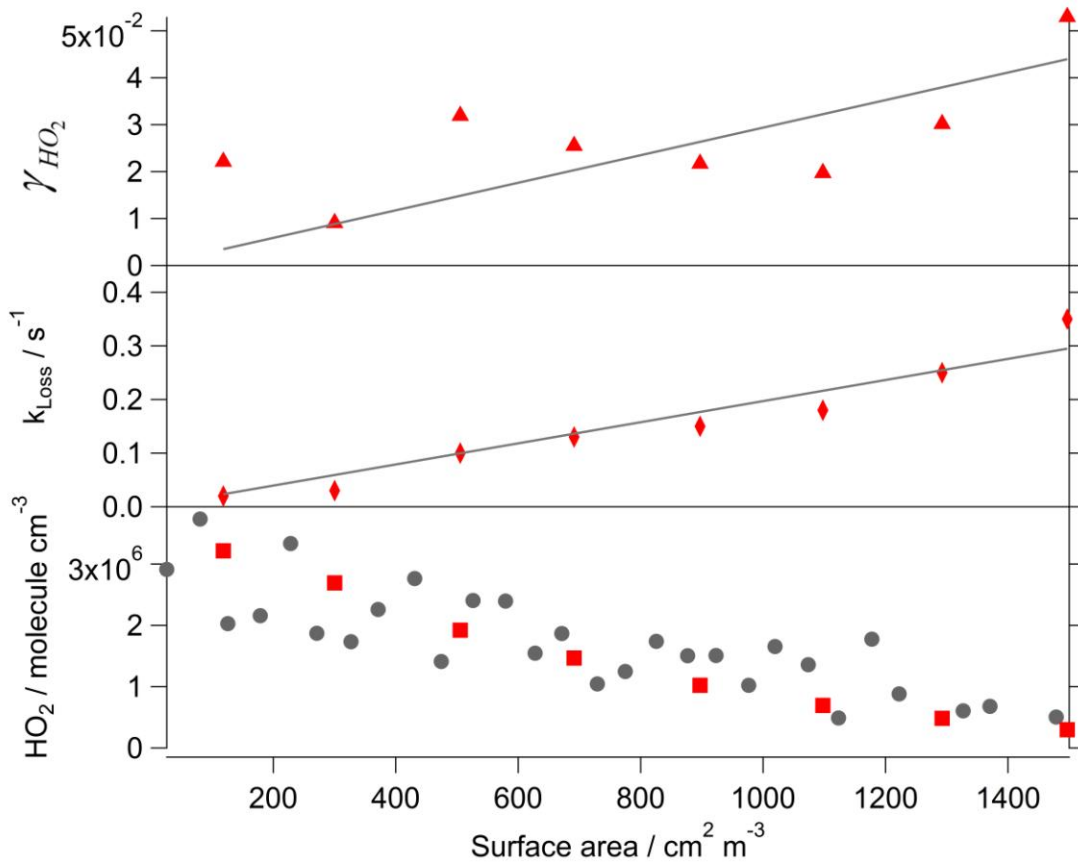


1

2 Figure 6, Upper panel. Average measured (solid red line) and simulated (dashed red line)
 3 diurnal profile of HO₂ concentrations outside of cloud events. The simulation is based on an
 4 expression originally determined by Carslaw et al. (1999) and described further in Sect. 2.2.
 5 The shading highlights the sensitivity of the model to $\pm 1\sigma$ changes in the CO and HCHO
 6 concentrations used as constraints.

7 Lower panel. Average measured (solid grey line) and modelled (dashed black and blue lines)
 8 diurnal profile of HO₂ concentration during cloud events. The model was run without (grey)
 9 and with (blue) a loss of HO₂ to cloud droplets equal to a first order loss rate of 0.1 s^{-1} . The
 10 shading highlights the sensitivity of the model to $\pm 1\sigma$ changes in the CO and HCHO
 11 concentrations used as constraints.

12

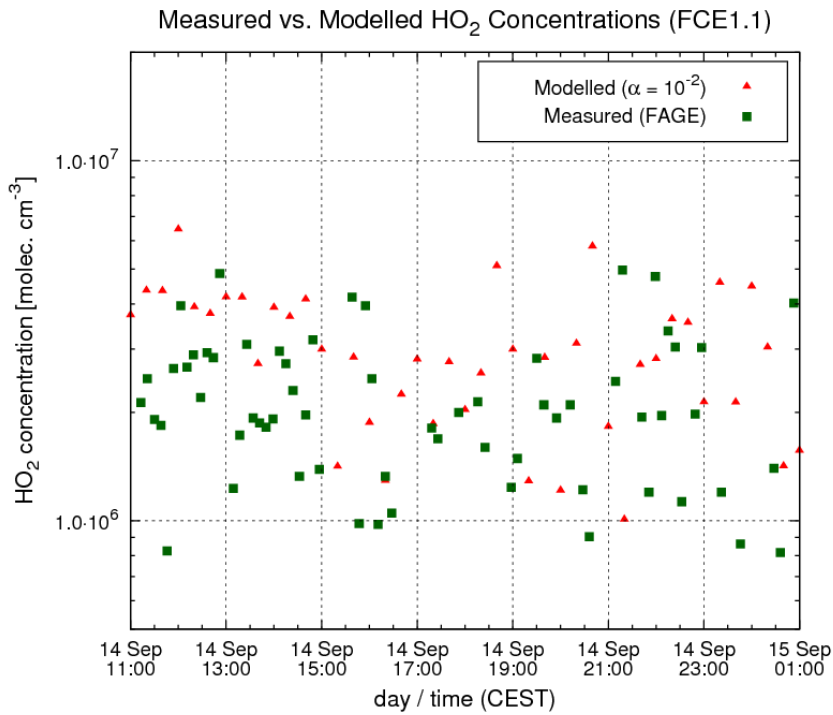


1

2 Figure 7, lower panel. The dependence of the measured HO₂ concentration (grey circles) and
 3 modelled HO₂ concentration with a variable first order loss (red squares) as a function of
 4 cloud droplet surface area.

5 Middle panel. The dependence of the first order loss term used in the model expression to
 6 best replicate the observed in-cloud HO₂ as a function cloud droplet surface area. The line of
 7 best fit being ($k_{Loss} = 2 \pm 0.1 \times 10^{-4} \times SA$).

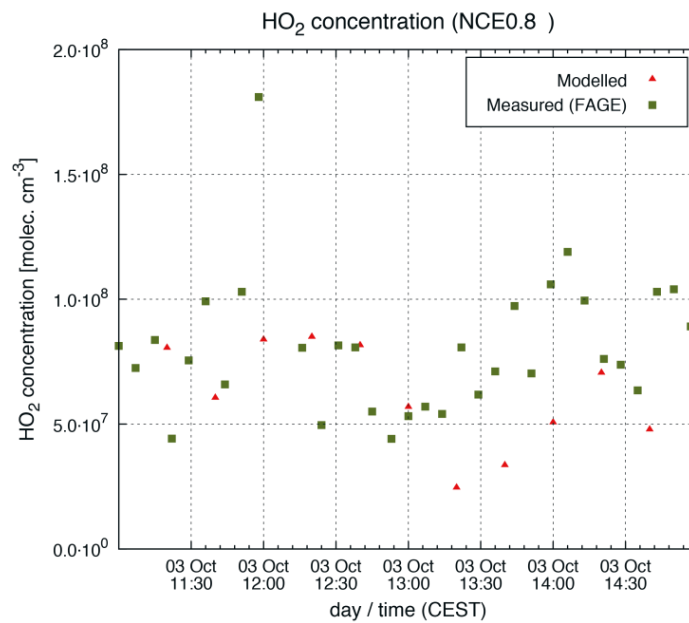
8 Upper panel. The dependence of γ_{HO_2} calculated using Eq. 7 as a function of cloud droplet
 9 surface area and constrained with the variable first order loss term as shown in the middle
 10 panel. The line of best fit being ($\gamma_{HO_2} = 2.9 \pm 0.5 \times 10^{-5} \times SA$).



1

2 Figure 8. Comparison of the measured (green squares) and modelled (red triangles), gas
 3 phase HO₂ concentrations at Mt. Schmücke site during cloud event FCE1.1 (14th, 15th Sept.
 4 2010 11:00-01:00 CEST).

5

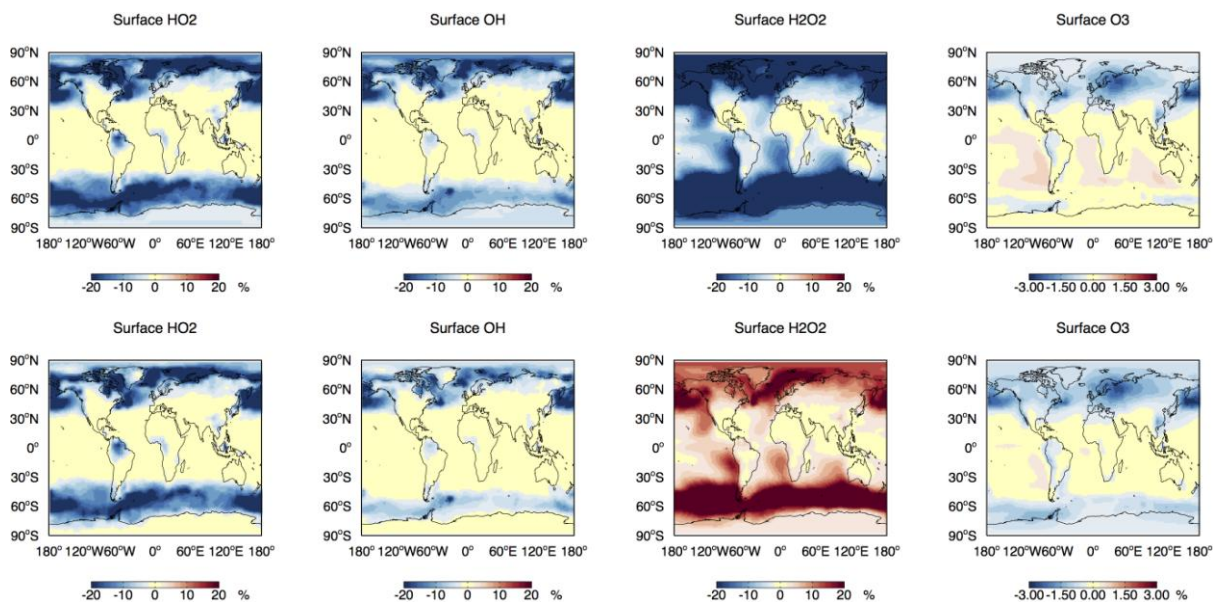


6

1 Figure 9. Comparison of the measured (green squares) and modelled (red triangles) gas phase
2 HO₂ concentrations at Mt. Schmücke site during the non-cloud event NCE0.8.

3

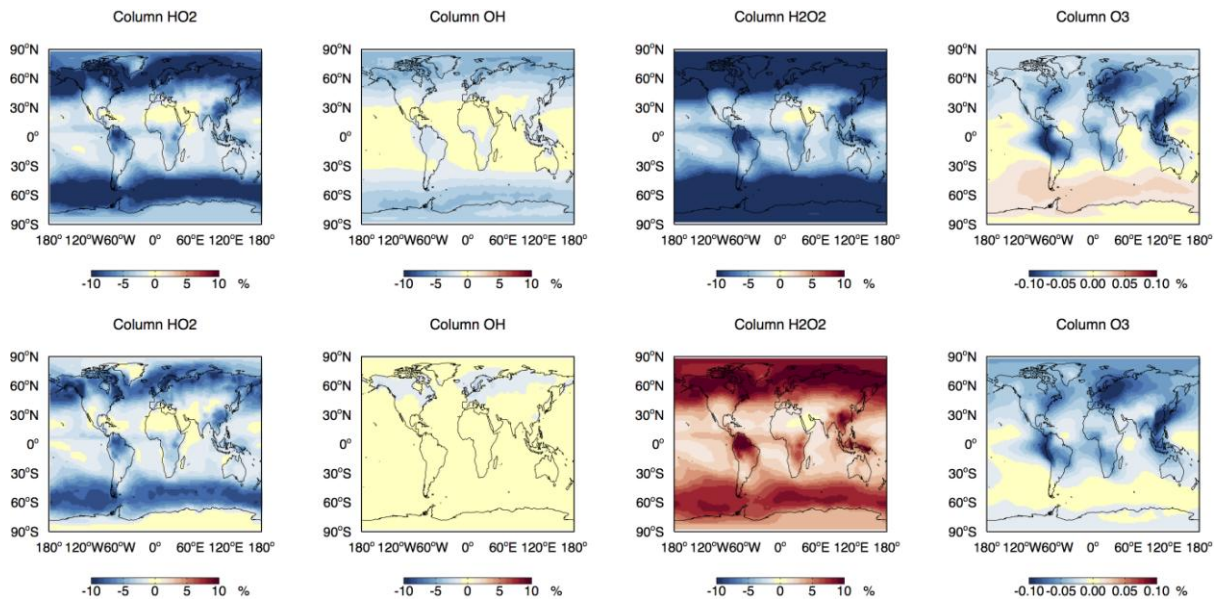
4



5

6 Figure 10. Annually average fractional change in surface HO₂, OH, H₂O₂ and O₃ with the
7 inclusion of HO₂ uptake into clouds leading to a) the production of H₂O and b) the production
8 of H₂O₂ assuming a cloud pH of 5 and the Thornton et al. (2008) parameterization.

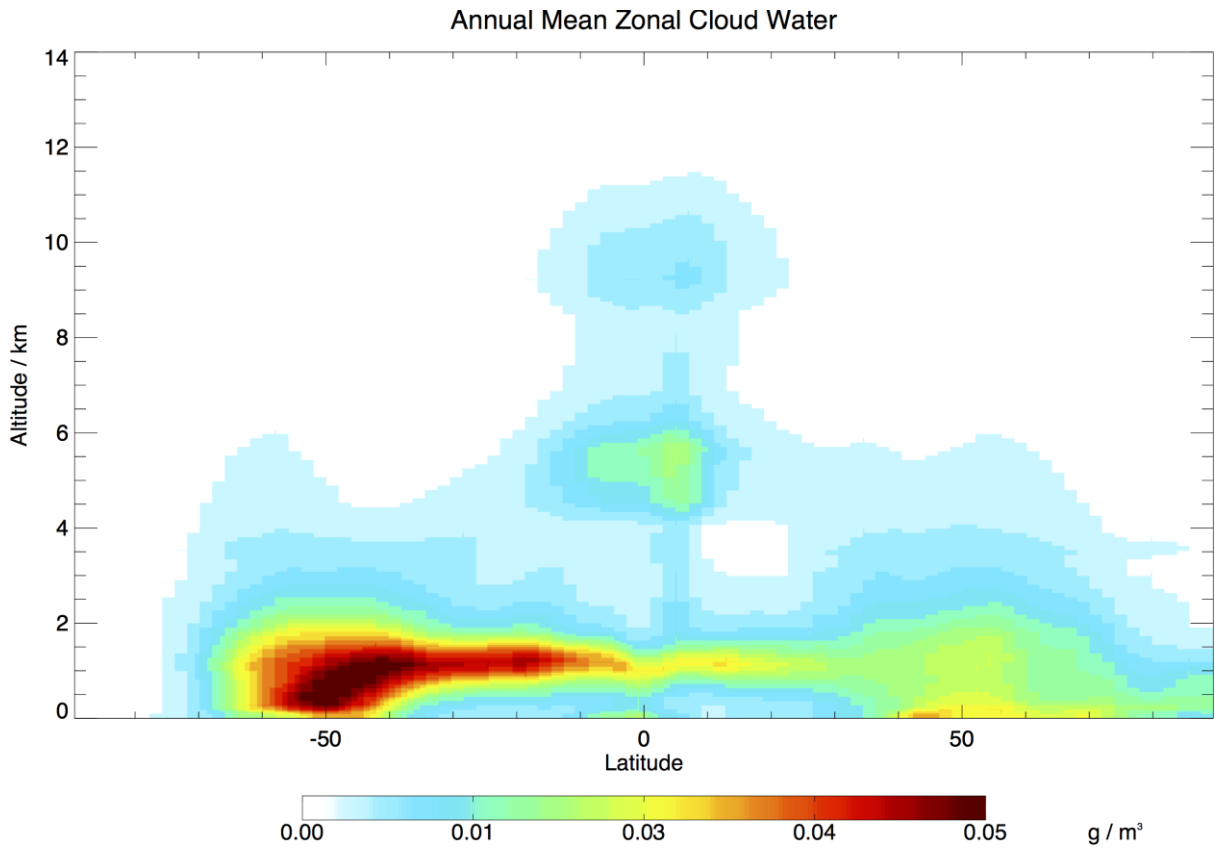
9



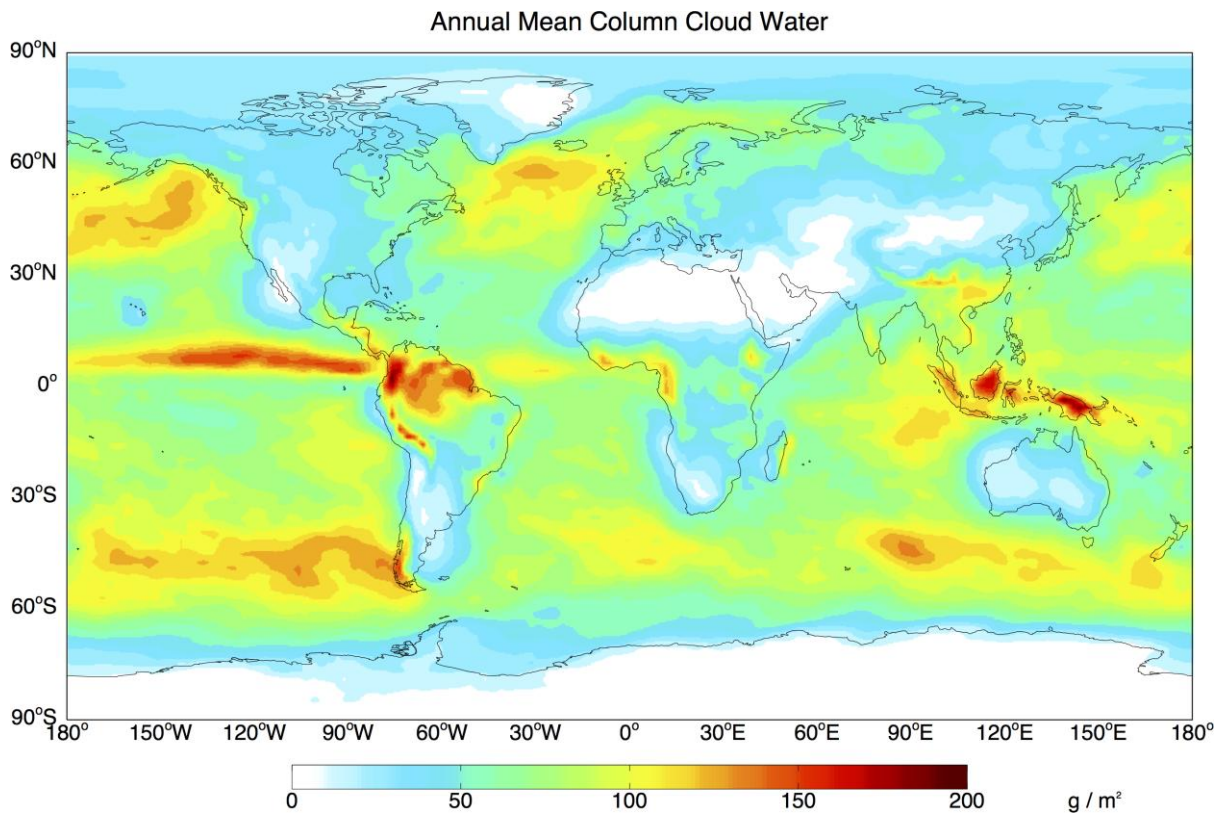
1
 2 Figure 11. Annually averaged fractional change in column HO_2 , OH , H_2O_2 and O_3 with the
 3 inclusion of HO_2 uptake into clouds leading to a) the production of H_2O and b) the production
 4 of H_2O_2 assuming a cloud pH of 5 and the Thornton et al. (2008) parameterization.

5

1



2



3

- 1 Figure 12. Annually averaged cloud water in the GEOS5 fields as a) a column total and b) a
- 2 zonal mean.